4.4 A NUMERICAL INVESTIGATION OF CONVECTIVE STORM EVOLUTION IN CASES OF MERGERS BETWEEN SQUALL LINES AND ISOLATED SUPERCELLS

Adam J. French* and Matthew D. Parker
North Carolina State University, Raleigh, North Carolina

1. INTRODUCTION

A considerable fraction of significant severe weather (damaging winds, large hail and/or tornadoes) tends to occur with organized convection in the form of quasi-linear convective systems (QLCSs or "squall lines") and supercell thunderstorms. Given the apparent threat posed by these systems, it is no surprise that they have each received a great deal of attention in the severe storms literature over the years, leading to an improved of understanding of both phenomena. However, these two convective modes are often studied in isolation, with a given study focusing on one mode or the other, despite the fact that they often occur in close proximity to one another (e.g. French and Parker 2008). This has left a gap in the knowledge base regarding how supercells and squall lines interact when they are present in close proximity to one another, and what these interactions might mean for the production of severe weather. The present paper looks to address part of this question, with an investigation of how isolated supercell thunderstorms merge with squall lines.

Past research on squall line-supercell mergers has focused primarily on documenting observed behaviors, particularly on the apparent relationship between the merger and tornadogenesis (e.g. Goodman and Knupp 1993; Wolf et al. 1996; Sabones et al. 1996; Wolf 1998). Little is known, however, about the storm-scale dynamics at work in these types of events. Perhaps the most detailed storm-scale analysis comes from the observational study of Goodman and Knupp (1993), who utilized mesonet data and visual observations to investigate the evolution of surface features associated with a squall line-supercell merger. They observed that the squall line's gust front was "distorted" in the vicinity of the merger with the supercell. They hypothesized that the distortion of the gust front may have been the result of its eastward advance being locally "blocked" by the surface meso-high associated with the supercell's outflow.

The possibility of the supercell in some way distorting the squall line's gust front is of interest as a slowing or weakening of the squall line in the vicinity of the merger was a common feature identified in recent observational work conducted by the present authors (French and Parker, submitted to *Weather and Forecasting*). Given the importance of lifting along the gust front to squall line maintenance and organization (e.g. Rotunno et al. 1988), determining how it evolves during the course of the merger is an important element in understanding these events. An initial investigation as to the processes at work that drive this weakening was presented by French and Parker (2010). In that study, the authors used convection-allowing (3 km horizontal grid spacing) Weather Research and Forecasting (WRF) model simulations to investigate two merger cases. Among their results, they found that the outflow produced by the supercell acted to locally weaken the gust front lifting along the squall line, leading to a decline in squall line intensity in the vicinity of the merger (Fig. 1). As the supercell merged with this weakened portion of the squall line, it became the new leading edge of the squall line, and thus continued to ingest favorable environmental air well after the merger (Fig. 2). The authors hypothesized that this continued source of favorable inflow was important to sustaining supercell structures within the merged system.

While these case-study simulations provided an initial look at the processes responsible for pre-merger squall line weakening, they do suffer from some drawbacks. First, the horizontal grid spacing of 3 km is fairly coarse in terms of resolving convective-scale features. As demonstrated by Bryan et al. (2003) horizontal grid spacings on the order of 100s of m are necessary to effectively simulation convective-scale processes, and thus higher resolution simulations would be desirable. Additionally, when running simulations in a case-study configuration, one is reliant on the grid-scale processes to develop the storms and structures of interest. While this often produced simulated structures that are

**Corresponding author address:* Adam J. French, Department of Marine, Earth, & Atmospheric Sciences, North Carolina State University, Campus Box 8208, Raleigh, NC 27695–8208. E-mail: ajfrench@ncsu.edu

more true to reality, it limits the opportunity to perform controlled experiments wherein features such as merger timing or location are explicitly controlled. Such experiments could be very useful in elucidating the details between different merger scenarios.

To address these shortcomings, the present study extends the work of French and Parker (2010) by running a series of high-resolution (500 m horizontal grid spacing) simulations of a squall line-supercell merger. The idealized framework of the present study allows us to test the effects of different merger locations along the squall line, and thus better understand the role that initial storm configuration plays in the ultimate storm organization. Additionally, the higher resolution of these simulations gives us the opportunity to further test the results of the case study simulations in a model configuration where convective-scale processes are actually resolved. The following section outlines the details of the idealized model configuration. Section 3 provides an overview of the basic simulations, followed by a discussion of the basic processes for the pre-merger weakening of the squall line in Section 4. Section 5 discusses the impact of shifting the merger location further south along the squall line. Finally, Section 6 provides some concluding remarks and explores some avenues for future work.

2. IDEALIZED SIMULATION SET-UP

This work utilized 3D idealized numerical model simulations using version 1.15 of the Bryan cloud model (CM1) described by Bryan and Fritsch (2002). We used a horizontal grid spacing of 500 m as a compromise in order to sufficiently resolve convective-scale processes while also keeping computing costs manageable given the 300 x 400 x 20 km grid necessary to simulate a squall line, supercell and merged system. The vertical grid spacing was stretched from 100 m at the surface to 250 m above z=2500 m. We employed open x- and y- lateral boundary conditions, free-slip upper and lower boundary conditions, and a Rayleigh damping layer above 14 km. In the interest of keeping these simulations as simple as possible radiative effects, surface friction and surface fluxes were all neglected. The simulations do include Coriolis forcing, applied to perturbation values only at a constant value of $f = 1 \times 10^{-4}\mathrm{s}^{-1}$ across the entire domain (i.e. an f-plane). This was included because initial tests revealed that it was necessary in order to produce the asymmetric structures (i.e. a dominant cyclonic line-end vortex at the north end of the squall line) similar to what was observed for real-world mergers. This is not surprising as the convergence of planetary vorticity has been shown by a number of studies to be important to the development of cyclonic mesoscale vortices over a wide range of scales (i.e. Skamarock et al. 1994; Weisman 1993; Atkins and St. Laurent 2009b). The present simulations used a horizontally homogeneous background environment (Fig. 3a), based on the idealized environment of Weisman and Klemp (1982), which has been widely used in the simulation of convective storms. The squall line was triggered using a 200 km long (y-dimension), 10 km wide, 3 km deep line thermal with a potential temperature perturbation of +2 K. Random noise of +/− 0.1 K was added to the thermal to help develop 3 dimensional structures along the line. A supercell was triggered 3 hours into the simulation using a single warm bubble positioned approximately 60 km ahead of the developing squall line.

Experience revealed that the main challenge in simulating a squall line-supercell merger lies with producing both convective modes simultaneously within a single simulation: in many cases a simulation that produced a reasonable supercell storm would not produce an effective squall line, and vice-versa. This stems from the long-understood concept that convective organization is strongly tied to the background environment, particularly the wind profile. Indeed, past idealized modeling studies have demonstrated that squall lines are favored in environments with strong unidirectional wind shear, generally isolated within the lowest 2-3 km AGL (e.g. Rotunno et al. 1988; Weisman et al. 1988; Weisman 1993; Weisman and Rotunno 2004; Bryan et al. 2006) while supercells are favored with strong deep-layer shear, particularly with a curved hodograph (e.g. Rotunno and Klemp 1982; Weisman and Klemp 1982; Weisman and Klemp 1984; Rotunno and Klemp 1985). In nature, the presence of environmental heterogeneity and strong linear forcing are often important to producing multiple modes in a localized region (e.g. French and Parker 2008). However, trying to include such heterogeneity in our idealized model would limit our ability to run controlled tests focused on the role that the storm merger is playing in convective evolution.

To address this issue, we initiated a squall line in an environment characterized by a favorable, unidirectional wind profile (Fig. 3a) and let it mature for three hours, essentially the time it took for the line to become steady. At this point, we output a restart file containing all of the run-time model fields, and modified the base-state wind profile within the restart file to resemble one more characteristic of a supercell environment, namely moderate (25 m s^{-1}) deep-layer shear and a low-level shear vector that veers with height (Fig. 3b). This was done by separating the original base-state wind profile from the perturbations that had developed in the course of running the 3-hour squall line simulation, introducing the new base-state wind profile, and then adding the original storm-induced perturbations back on to the new wind profile, as illustrated schematically in Fig. 4. In doing this we were able create a more favorable environment for supercells, while still maintaining the physical perturbations to the wind and thermodynamic fields produced by the squall line. The base state thermodynamic profile was left untouched; the small changes in values of CAPE and CIN between Figs. 3a and b are perturbations solely due to the presence of the squall line. Once the modifications were complete, we restarted the simulation using the modified restart file, and triggered the supercell ahead of the squall line with a warm bubble.

We ran three primary simulations using this method, which we have termed "base-state substitution". The first simulation consists of a squall line initiated by the line thermal and permitted to evolve without the addition of the modified environment. This is intended as a baseline to help evaluate the impacts of adding the stronger wind shear profile on the squall line, and will be referred to hereafter as the "BASE" simulation. The second simulation uses the same set-up as BASE, but adds the wind profile modification after 3 hours and is intended to isolate the effects of the stronger shear environment on the squall line. It will be referred to as the "NOMERGER" simulation. Finally, the third simulation includes the modifications of the NOMERGER simulation, and also adds a +1 K warm bubble 60 km ahead of the squall line when the simulation is restarted, triggering an isolated supercell that will eventually merge with the squall line. This will be referred to as the “MERGER” simulation.

The effects of changing the base state wind profile are summarized in Fig. 5. The top panels (a-e) illustrate the evolution of a squall line in the unchanged environment of the BASE simulation, and the bottom panels (f-j) illustrate a squall line in the NOMERGER simulation, where the modified wind profile is added 3 hours (180 min.) into the simulation (e.g. between panels g and h). The simulations are identical for the first three hours (Fig. 5a-b, f-g) and remain quite similar for the first 10-15 minutes following the restart time (Fig. 5c, h). However, by approximately 20 minutes after the new environment is introduced the squall line in the modified environment (Fig. 5i) starts to intensify compared to the one in the base state simulation (Fig. 5d). After an hour, the modified squall line (Fig. 5j) has begun to develop bow echo characteristics, and has accelerated eastward compared to the base state squall line (Fig. 5e). Thus the primary impact of adding the stronger wind profile is that the simulation produces a stronger squall line, as would be expected in a stronger-shear environment (e.g. Weisman et al. 1988; Weisman 1993). This test reassures us that the method provides an effective transition from a squall line to supercell wind profile, with no unphysical noise or detrimental effects to the simulated storms. Furthermore, by altering the environment instantaneously we are able to do so in a controlled manner. This allows us to study the impact of the storm merger in isolation, with the confidence that any changes in storm behavior are a direct result of the merger. If we had used a more gradual means of changing the wind profile, such as some type of forcing over time, or a horizontally varying wind, it would be challenging to isolate the changes in storm evolution owing to the merger from those owing to the changing wind profile.

3. OVERVIEW OF SIMULATIONS

The early evolution of the NOMERGER simulation is characterized by a quasi-two-dimensional squall line as shown in Fig. 5f-g. Once the stronger wind profile is introduced after 3 hours of simulation time, the squall line rapidly intensifies with an unbroken region of 40+ dBZ simulated radar reflectivity extending from y = 90 km to y = 215 km (Fig. 6a). The line continues to intensify as the simulation progresses, beginning to exhibit classic bow echo structure in the simulated reflectivity field by t = 245 min. (Fig. 6b). This bowing increases with time, as other hallmarks of bow echo structure (e.g. Weisman 1993) begin to materialize including bookend vortices and a strong elevated rear-inflow jet (Fig. 6d-f). Eventually the squall line develops an asymmetric structure with a dominant cyclonic vortex at its north end (Fig. 6f) owing to the presence of Coriolis forcing in the simulation (e.g. Davis and Weisman 1994; Skamarock et al. 1994). The development of a large bow echo after the vertical wind shear increase is consistent with past studies on the environments of bow echoes (e.g. Weisman et al. 1988; Weisman 1993), and indicates that the merger is not a necessary condition to develop a bow echo in this environment.

The squall line in the MERGER simulation begins in the same manner as that in the NOMERGER simulation, and the two squall lines are largely identical through approximately the first 4 hours of the simulation (c.f. Figs 6a-b and 7a-b). The supercell initiated by the warm bubble at t = 180 minutes evolves into a classic supercell with hook echo features and a well-developed mesocyclone (Fig. 8a-d) prior to the merger. The merger begins at approximately t = 265 minutes, as the squall line overtakes the supercell along its rear flank (Fig. 7c). At this point, radar reflectivity values begin to decline to the north of the merger location (Fig. 7b-d), consistent with observations of squall lines weakening north of the merger location. As the merger progresses, several reflectivity structures common to observed mergers begin to emerge. These include "Y"-shaped, and "S"-shaped reflectivity patterns early in the merger (Fig. 7b-c and d, respectively), followed by "reflectivity swirl" and "comma echo" configurations as the bow echo becomes predominant (Fig. 7e-f). These features were all common in observed merger events (French and Parker, submitted to *Weather and Forecasting*). Also consistent with a number of observed cases, as the merger concludes the remnant supercell becomes the northern end of the squall line as it subsequently evolves into a bow echo (Fig. 7e-f). This bow echo persists through the remainder of the simulation.

Given the many qualitative similarities between the structures in the MERGER simulation, and those found in observed cases, we are confident that this simulation is effectively capturing the impacts of a squall line-supercell merger. With this in mind, we will now move forward with a more in depth discussion of the evolution of the squall line cold pool during the course of the merger.

4. COLD POOL EVOLUTION

Given that the cold pool is central to squall line dynamics, understanding how it evolves during the course of a merger event is key to determining why the squall line behaves as it does. One might intuitively think that the large cold pool associated with the squall line would effectively overwhelm the supercell, cutting off its inflow and causing it to weaken following the merger. However, based on the observations of a squall line's gust front being "distorted" during a merger by Goodman and Knupp (1993), not to mention the repeated observations of apparent sustained supercell structures post-merger detailed noted by French and Parker (submitted to *Weather and Forecasting*), this does not appear to be the case. To understand why, we will now look in detail at the evolution of the squall line's cold pool in our MERGER simulation.

Post-merger, the cold pool in the MERGER simulation appears to weaken considerably compared to that in the NOMERGER run. This is illustrated in a difference plot comparing the MERGER and NOMERGER simulations 30 minutes after the merger begins (Fig. 9). In the region where the merger occurred (between y = 170 and 190 km, Fig. 9) the MERGER simulation cold pool is generally 3-5 K warmer than the NOMERGER cold pool. This suggests a significant weakening of the cold pool associated with the merger, and corresponds to lower simulated reflectivity values seen north of the merger in Fig. 7c-d . This weakening appears to be the direct result of an interaction between the system's cold pool and the pre-line supercell outflow[1]. As the supercell develops ahead of the squall line, it begins to produce cold outflow along its rear flank (Fig. 10a). The squall line's cold pool eventually encounters this spreading supercell outflow (black arrow, Fig. 10b), which initiates a weakening trend in the squall line's gust front. As the comparatively cooler air associated with the supercell's outflow encounters the squall line's gust front, the cross-gust front potential temperature gradient begins to weaken (e.g. black arrows, Fig. 10b-c). Over time, this gradient weakens further, over a larger region (Fig. 10d), eventually becoming non-existent by t = 275 min. (dashed oval in Fig. 10e). At this point, the gust front associated with the supercell outflow effectively becomes the new leading edge of the system's cold pool in the vicinity of the merger.

The weakening of the gust front temperature gradient impacts the squall line in two ways. First, a weaker temperature difference across the gust front means that the density difference driving gust front motion is weaker, resulting in a slower forward motion of the gust front. This is evident in Fig. 10b-d, as the portion of the squall line's gust front interacting with the supercell outflow begins to lag behind the segment that is farther south. This diminished temperature gradient is also detrimental to low-level lifting associated with the gust front. The cross-gust front temperature gradient is responsible for creating a pressure perturbation that drives upward motion at the leading edge of the gust front, forcing inflowing air to ascend as it reaches the gust front interface. As this temperature gradient weakens, so too does the cold pool's ability to force vertical motion at its leading edge (e.g. Fig. 10f-j). This is

[1]The outflow from the supercell obviously constitutes a cold pool of its own. However, for the purposes of this discussion and the sake of clarity, "cold pool" will refer to the squall line's cold pool, and later that of the merged system, while "supercell outflow" will refer to the cold air associated with the supercell while ahead of the squall line.

evident as a decline (black arrows, Fig. 10h-i) and eventual dissipation (dashed oval, Fig. 10j) of the otherwise continuous slabular ascent initially associated with the squall line north of the merger.

Along with the weakening gust front lifting, the supercell's outflow also weakens the squall line by locally cutting off its supply of high-θ_e inflow in the vicinity of the merger. Early in the simulation the squall line is being sustained by 2 km deep layer of high-θ_e inflow along the length of its gust front (Fig. 11a, d). As the spreading outflow associated with the supercell encounters the squall line, it begins to limit the amount of this inflow that reaches the squall line (Fig. 11b). Initially, the supercell's outflow is comparatively shallow, and an elevated region of high-θ_e parcels continues to fuel the squall line (Fig. 11e). However, as the supercell's outflow deepens over time, this elevated layer is eroded, and the parcels being lifted by the squall line have comparatively lower values of θ_e (Fig. 11f). These lower-θ_e parcels have less CAPE, and contribute to the overall decline in convection along the squall line in the vicinity of the merger.

The combined effects of a cessation of high-θ_e inflow and diminished low-level lifting result in the squall line weakening north of the merger, and the merged supercell becoming the new northern end of the squall line. At the same time, the presence of the supercell's outflow appears to be the key to the supercell being sustained through the merger (instead of being overwhelmed by the squall line's cold pool). As this outflow from the supercell interacts with the squall line and weakens the cross-gust front temperature gradient, the squall line's gust front effectively stalls, and the gust front associated with the supercell becomes the new leading edge of the merged system. As a result, the supercell's updraft and mesocyclone continue to ingest environmental air, sustaining these structures during the early stages of the merger. These behaviors were common in real-world cases with the eventual weakening of the northern end of the squall line or at least temporary "breaks" in the squall line observed in most cases. Furthermore, the structures associated with the supercell could often be tracked throughout the merger, indicating that it was being sustained. Based on the results presented in this section, it would appear that the weakening of the squall line's cold pool by the supercell's outflow is directly responsible for both the weakening of the squall line, and the sustenance of the supercell.

5. SENSITIVITY TO MERGER LOCATION

To investigate the role that merger location plays, three additional simulations were run wherein the bubble used to initiate the supercell was moved progressively further south as shown in Fig. 12a-d. This resulted in bubbles placed at y=150, y=130, and y=90 km which will be referred to as the Y150, Y130, and Y90 runs respectively (for reference in the MERGER simulation the bubble was placed at y=170 km). These locations represent shifts of 20, 40, and 80 km from the original bubble location in the MERGER simulation (i.e. the distance doubles for each test).

As the location of the merger moves south, it has a progressively smaller impact on the squall line in terms of weakening north of the merger and bow echo development south of the merger, two of the main characteristics identified in the MERGER simulation. In the Y150 simulation, the post-merger bow echo appears fairly similar to that in the MERGER simulation (c.f. Fig. 13a and b), just shifted further south. There is also a general weakening trend north of the merger, although it is not nearly as pronounced as in the MERGER simulation, with a large area of $>$ 40 dBZ simulated radar reflectivity remaining north of y =150 km. The Y130 simulation, produces a more dramatic departure from the MERGER simulation, with weaker bowing, and the squall line being largely sustained north of the merger location (Fig. 13c). Finally, in the Y90 simulation, there is no clear bowing associated with the merger, and the squall line is largely unchanged north of the merger (Fig. 13d).

The apparent maintenance of the squall line north of the merger location in the Y150, Y130 and Y90 simulations appears to result from the squall line's cold pool remaining strong throughout the merger. Recalling the discussion from the previous section, in the MERGER simulation, the weakening of the squall line north of the merger appears to be a direct result of a diminished cold pool intensity (e.g. Fig. 14a). As the merger is moved south, however, this weakening is not as pronounced in the Y150 simulation (Fig. 14b) and is largely absent in the Y130 and Y90 simulations (Fig. 14c, d). This is likely because as the merger is shifted south, it occurs closer to the strongest (i.e. coldest, deepest) part of the squall line's cold pool. As a result, the squall line's cold pool is less apt to be influenced by the weaker outflow associated with the supercell (Fig. 14). This suggests that the weakening trend observed at the north end of the squall line in the MERGER simulation is at least partially a function of the merger occurring close to the north end of the line.

The location of the merger also has an influence on the production of strong surface winds and low-level vertical vorticity in the merged system. Once again, the Y150 simulation behaves similarly to the MERGER simulation, with the merged system producing a large region of strong surface winds (Fig. 15a-b). However, as the merger is shifted south, the extent of this swath is much less pronounced, with the Y130 and Y90 simulations producing isolated pockets of severe surface winds (Fig. 15 c, d). Initial results suggest that the large swaths of severe winds in the MERGER and Y150 simulations owe their existence to enhanced surface outflow, however additional analysis is underway to evaluate the role that mesovortex circulations may contribute to these enhanced winds, or the more localized regions of strong winds in the Y130 and Y90 simulations (e.g. Trapp and Weisman 2003; Wakimoto et al. 2006; Atkins and St. Laurent 2009a). The changes in vorticity evolution are evident in the time series shown in Fig. 16a-d. The Y150 simulation produces a peak in vertical vorticity following the merger that is much longer lived than that in the MERGER simulation (c.f. Fig. 16a-b), albeit slightly weaker in magnitude. Further south both the Y130 and Y90 simulation also produce increases in vertical vorticity following the merger (Fig. 16c, d), however these are comparatively weak and/or short-lived. In fact, in the Y90 simulation the strongest vertical vorticity occurs with the isolated supercell prior to the merger (t = -30 - t = -10 min., Fig. 16d), perhaps owing to a later merger time in this simulation.

The decline in vertical vorticity seen as the merger is shifted south is not all that surprising, given the larger-scale vorticity structure associated with squall lines. As shown by Weisman (1993) mature bow echoes are characterized by counter-rotating bookend vortices, with a cyclonic vortex at the north end of the line and an anti-cyclone vortex at the south end. In environments with Coriolis forcing, such as the present simulations, the northern cyclonic will dominate due to the convergence of planetary vorticity (e.g. Weisman 1993; Davis and Weisman 1994; Skamarock et al. 1994). In the present simulations, the mergers that occur toward the north end of the line (e.g. MERGER, Y150) appear to benefit from this enhanced cyclonic vorticity, resulting in the large values of low-level vertical vorticity post-merger (Fig. 16a, b). Meanwhile, the diminished vertical vorticity observed with the mergers further south (e.g. Y130, Y90, Fig. 16c, d), would appear consistent with an environment characterized by weakly anti-cyclonic vertical vorticity, as is found at the south end of a mature squall line.

Thus, the location of the merger along the squall line appears to play an important role in the ultimate squall line evolution. For mergers north of the center point of the squall line (e.g. MERGER, Y150) more pronounced bowing occurs and the squall line weakens more considerably north of the merger. These locations also appear to favor the development of strong low-level vertical vorticity and severe surface winds. For mergers that occur near or south of the center-point of the squall line (e.g. Y130, Y90), the impact of the merger is much more localized and the squall line is better maintained north of the line. Additionally, these situations are characterized by weaker, shorter lived increases in low-level vertical vorticity, and more localized damaging surface winds. All told, these results suggest that merger location may be an important delineator between different merger evolutions that are observed in nature, along with differences in the observed sensible weather. This may have important implications for severe weather forecasting, as this may indicate a varying severe weather threat depending on the merger location.

6. SUMMARY AND CONCLUSIONS

Idealized model simulations have been performed to examine the processes responsible for some commonly observed behaviors associated with squall line-supercell mergers, particularly, the oft-observed pre-merger weakening of the squall line. In-depth analysis of a simulation that captures a merger (the MERGER simulation) revealed that that this weakening is driven by an interaction between surface outflow produced by the supercell and the squall line's gust front. As the outflow impinges upon the squall line's gust front, the cross-gust front temperature gradient is weakened, leading to a decline in low-level gust front lifting. This results in an overall decline in convective activity associated with the squall line along and north of the merger location, precluding a re-invigoration of the squall line's cold pool. This weakening causes the merged supercell to become the new north end of the squall line in the MERGER simulation, allowing it to continue to ingest favorable environmental air following the merger. These findings are in line with earlier coarse-resolution case study simulations (French and Parker 2010) as well as past observational work (Goodman and Knupp 1993). We hypothesize that this may be important to sustaining the merged supercell's intensity and low-level rotation post-merger. Sensitivity tests wherein the merger location was moved progressively further south along the squall line indicate that the morphology of the merged system is sensitive to the location of the merger. In particular, as the location is shifted south, the merged supercell becomes increasingly weaker and shorter lived. This appears to be due to the maintenance of the squall line's cold pool north of the merger causing a re-generation of the cold pool in the vicinity of the merger, leading to the merged supercell being cut off from its environmental inflow sooner.

The identification of the cold pool weakening mechanism is but a first step in better understanding these types of merger events. Additional analysis of the present simulations is on-going to examine the details of low-level rotation before and after the merger. Furthermore, future simulations are planned to investigate the sensitivity of post-merger behavior to other features such as the background environment and storm maturity at the time of merger.

Acknowledgments

The authors would like to thank the members of the Convective Storms Group at NC State University, particularly Casey Letkewicz and Johannes Dahl for thoughtful discussion and assistance in the course of this work. We would also like to thank George Bryan for developing and supporting CM1, and making it available for research use. High performance computing resources were provided by OIT High Performance Computing at NC State and the Renaissance Computing Institute in Chapel Hill, NC. This work is funded by NSF grants ATM-0552154 and ATM-0758509.

References

Atkins, N. T. and M. St. Laurent, 2009a: Bow echo mesovortices: Part I: Processes that influence their damaging potential. *Mon. Wea. Rev.*, **137**, 1497–1513.

———, 2009b: Bow echo mesovortices: Part II: Their genesis. *Mon. Wea. Rev.*, **137**, 1514–1532.

Bryan, G. H. and M. J. Fritsch, 2002: A benchmark simulation for moist nonhydrostatic numerical models. *Mon. Wea. Rev.*, **128**, 3941–3961.

Bryan, G. H., J. C. Knievel, and M. D. Parker, 2006: A multimodel assessment of RKW Theory's relevance to squall-line characteristics. *Mon. Wea. Rev.*, **134**, 2772–2792.

Bryan, G. H., J. C. Wyngaard, and M. J. Fritsch, 2003: Resolution requirements for the simulation of deep moist convection. *Mon. Wea. Rev.*, **131**, 2394–2416.

Davis, C. A. and M. L. Weisman, 1994: Balanced dynamics of mesoscale vortices produced in simulated convective systems. *J. Atmos. Sci.*, **51**, 2005–2030.

French, A. J. and M. D. Parker, 2008: The initiation and evolution of multiple modes of convection within a meso-alpha scale region. *Wea. Forecasting*, **23**, 1221–1252.

French, A. J. and M. D. Parker, 2010, Numerical simulations of interactions between squall lines and supercells. Preprints, *25th Conf. Severe Local Storms*, Denver, CO, Amer. Meteor. Soc.

Goodman, S. J. and K. R. Knupp, 1993, Tornadogenesis via squall line and supercell interaction: The November 15, 1989, Huntsville, Alabama, tornado. *The Tornado: Its Structure, Dynamics, Prediction, and Hazards*. No. 79, Amer. Geophys. Union.

Rotunno, R. and J. B. Klemp, 1982: The influence of the shear–induced pressure gradient on thunderstorm motion. *Mon. Wea. Rev.*, **110**, 136–151.

———, 1985: On the rotation and propagation of simulated supercell thunderstorms. *J. Atmos. Sci.*, **42**, 271–292.

Rotunno, R., J. B. Klemp, and M. L. Weisman, 1988: A theory for strong, long–lived squall lines. *J. Atmos. Sci.*, **45**, 463–485.

Sabones, M., E. M. Agee, and M. Akridge, 1996, The Pulaski county and West Lafayette, Indiana tornadoes, 26-27 April 1994: A case of supercell (mesocyclone) and squall line bow-echo interaction. Preprints, *18th Conf. Severe Local Storms*, San Francisco, CA, Amer. Meteor. Soc.

Skamarock, W. C., M. L. Weisman, and J. B. Klemp, 1994: Three-dimensional evolution of simulated long-lived sqaull lines. *J. Atmos. Sci.*, **51**, 2563–2584.

Trapp, R. J. and M. L. Weisman, 2003: Low-level mesovortices within squall lines and bow echoes. part II: Their genesis and implications. *Mon. Wea. Rev.*, **131**, 2804–2823.

Wakimoto, R. M., H. V. Murphey, C. A. Davis, and N. T. Atkins, 2006: High winds generated by bow echoes. part II: The relationship between the mesovortices and damaging straight-line winds. *Mon. Wea. Rev.*, **134**, 2813–2829.

Weisman, M. L., 1993: The genesis of severe, long–lived bow echoes. *J. Atmos. Sci.*, **50**, 645–670.

Weisman, M. L. and J. B. Klemp, 1982: The dependence of numerically simulated convective storms on vertical wind shear and buoyancy. *Mon. Wea. Rev.*, **110**, 504–520.

———, 1984: The structure and classification of numerically simulated convective storms in directionally varying wind shears. *Mon. Wea. Rev.*, **112**, 2479–2498.

Weisman, M. L., J. B. Klemp, and R. Rotunno, 1988: Structure and evolution of numerically simulated squall lines. *J. Atmos. Sci.*, **45**, 1990–2013.

Weisman, M. L. and R. Rotunno, 2004: "A theory for strong long–lived squall lines" revisited. *J. Atmos. Sci.*, **61**, 361–382.

Wolf, P. L., 1998: WSR-88D radar depiction of supercell-bow echo interaction: Unexpected evolution of a large, tornadic "comma-shaped" supercell over eastern Oklahoma. *Wea. Forecasting*, **13**, 492–504.

Wolf, R., R. Przybylinski, and P. Berg, 1996, Observations of a merging bowing segment and supercell. Preprints, *18th Conf. Severe Local Storms*, San Francisco, CA, Amer. Meteor. Soc.

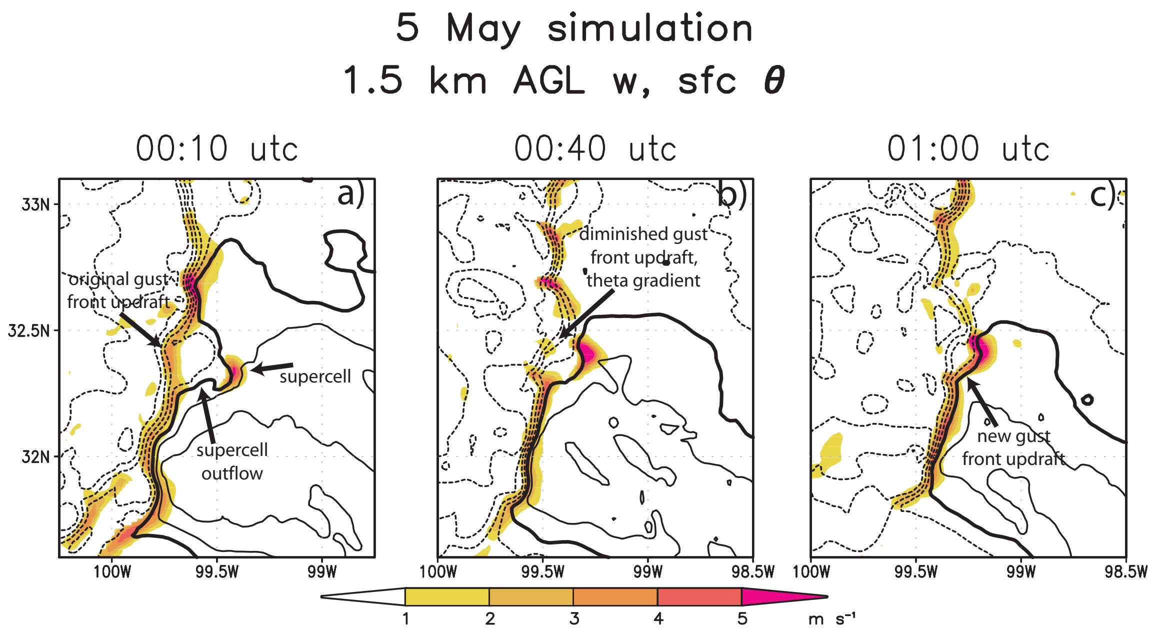

Figure 1: Time evolution of 1.5 km AGL w (m s^{-1}, shaded as shown) and surface potential temperature (K, contoured every 1 K, values greater than 300 K (heavy contour) are solid, less than 300 K dashed) from a 3 km WRF simulation of the 5 May 1995 merger case at (a) 0010, (b) 0040 and (c) 0100 UTC .

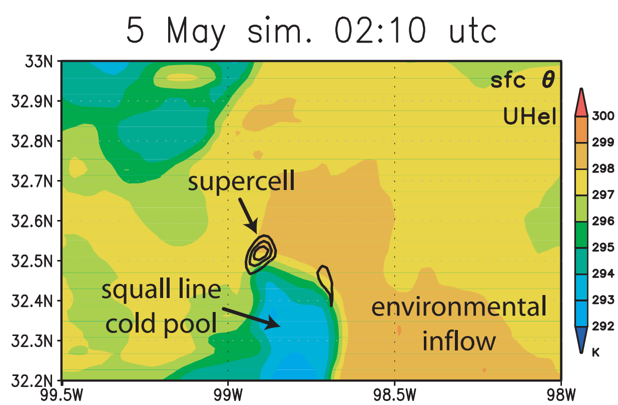

Figure 2: Surface potential temperature (shaded as shown) and updraft helicity (positive values contoured every 250 m^2s^{-2}) from a 3 km WRF simulation of the 5 May 1995 merger case at 0210 UTC.

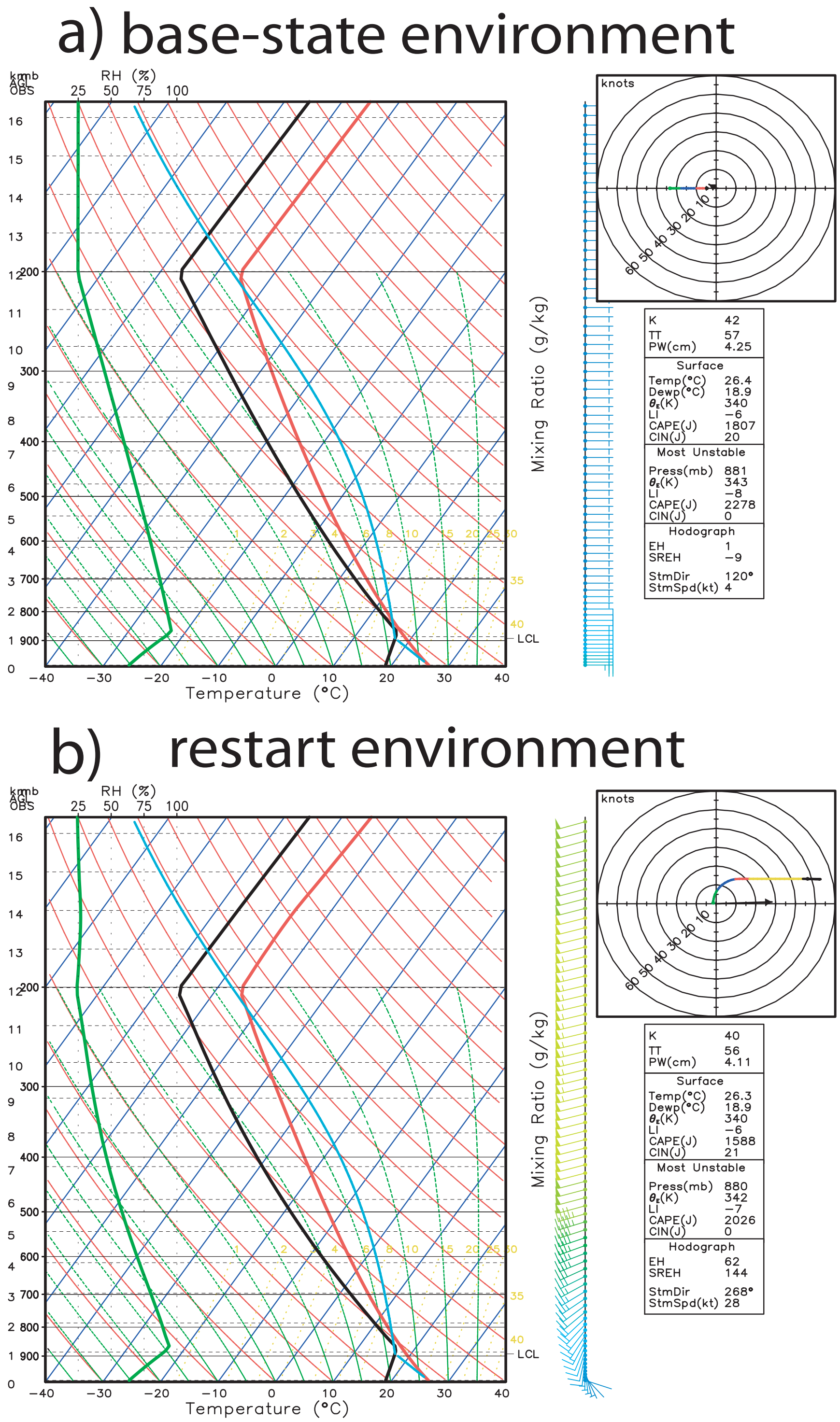

Figure 3: Skew-T log-P diagram of temperature, dew point temperature and lifted parcel path, wind profiles and hodographs (kts) for (a) the base-state squall line environment and (b) the supercell environment added 3 hours into the simulation. Color coding on the hodograph denotes various height layers as follows: green: 0-1 km, blue: 1-2 km, red: 2-3 km, yellow 3-6 km, and black 6km- model top. Wind barbs are in knots with a half barb = 5 knots, full barb = 10 knots, and flag = 50 knots.

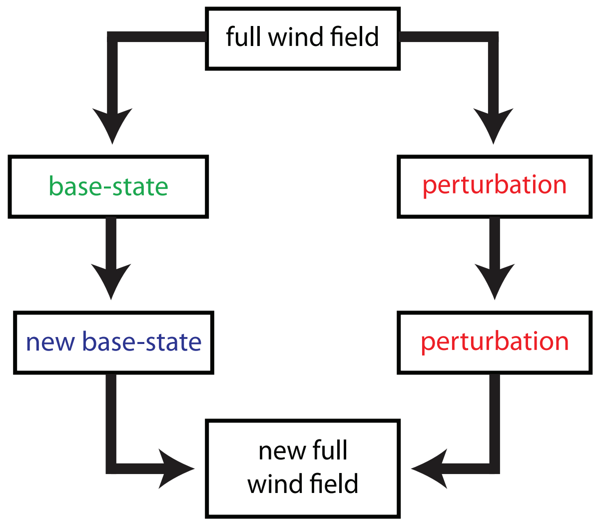

Figure 4: Schematic diagram illustrating the base-state substitution method described in the text.

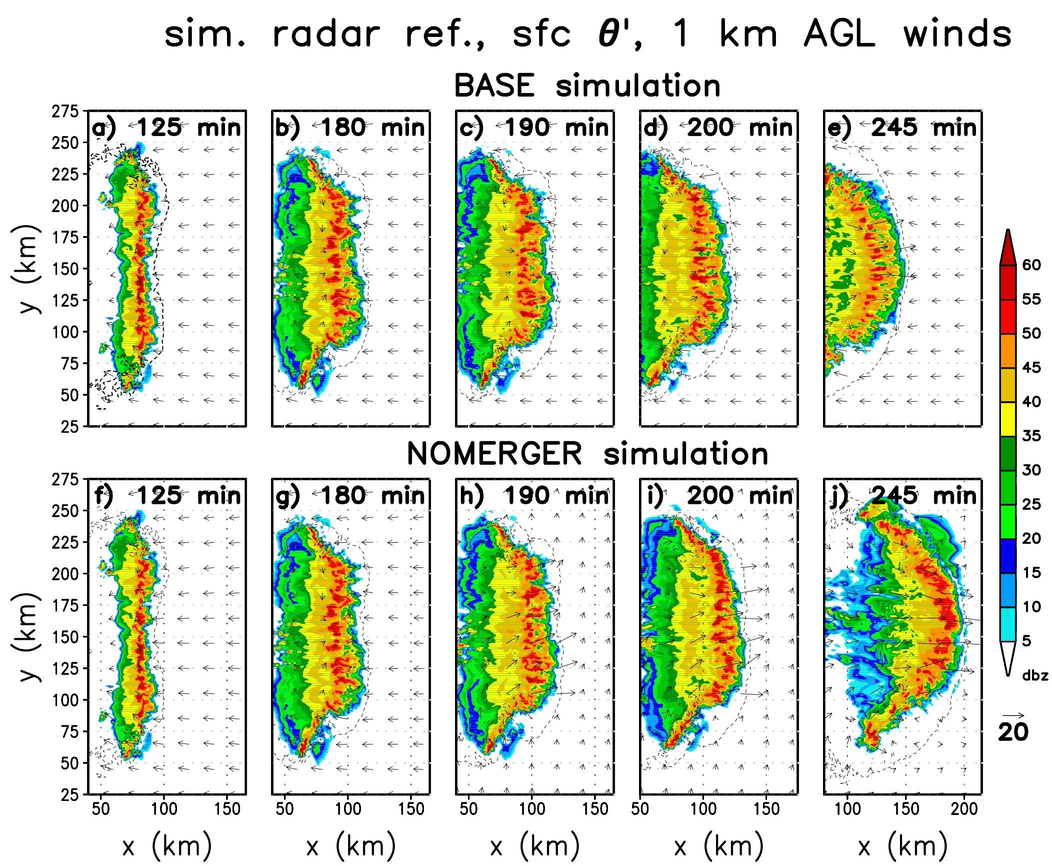

Figure 5: Simulated radar reflectivity (dBZ), 1 km AGL winds (m s^{-1} , representative vector at the lower-right), and -1 K surface potential temperature perturbation between t = 125 and 245 minutes for (a)-(e) a squall line simulation using the initial base-state environment and (f)-(j) a squall line simulation wherein the environment is modified after 3 hours, as discussed in the text.

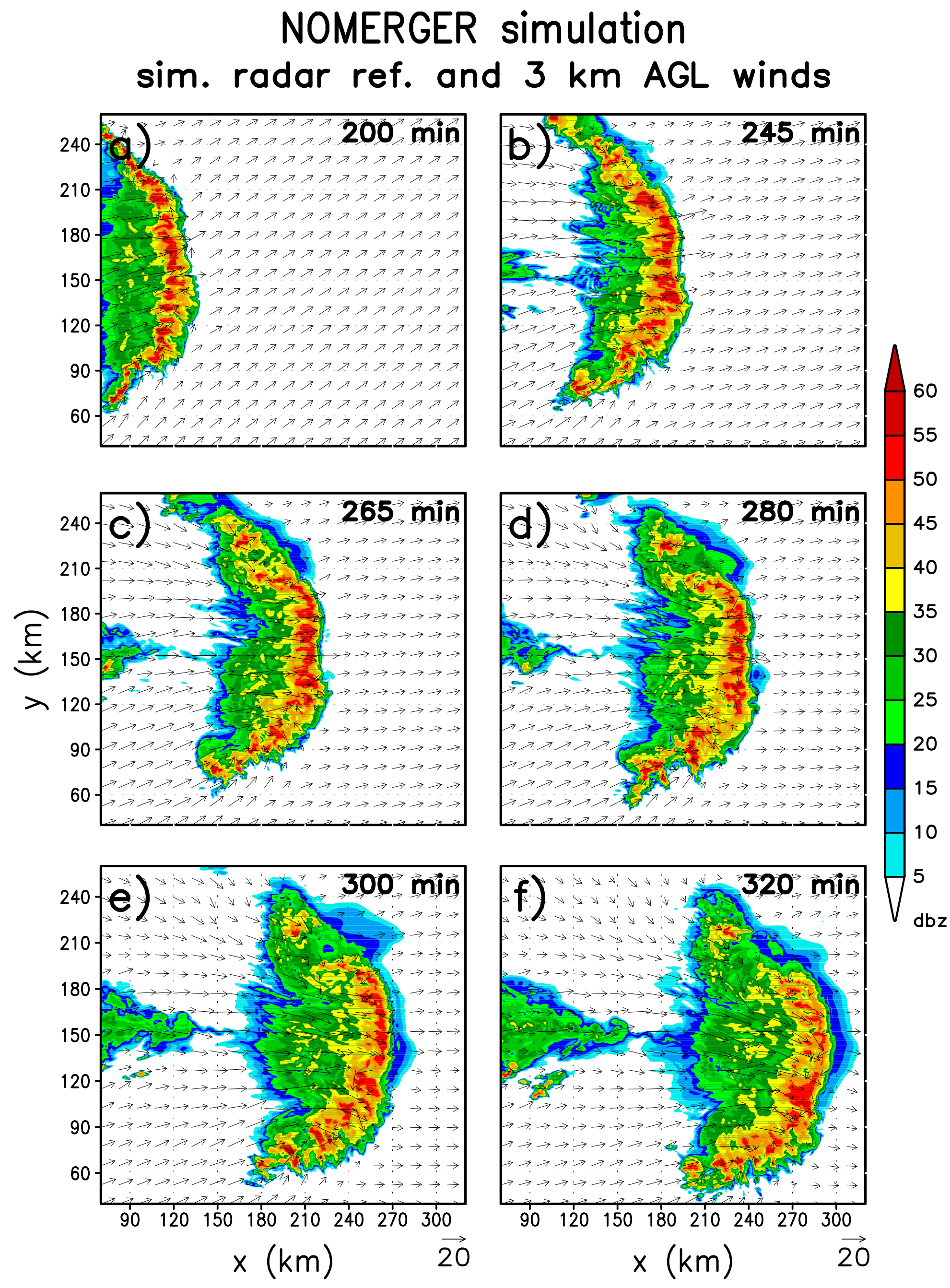

Figure 6: Simulated radar reflectivity (dBZ, shaded as shown) and 1 km AGL winds (m s^{-1}, representative vector at lower right of panels e and f) at (a) 200 (b) 245 (c) 265 (d) 280 (e) 300 and (f) 320 minutes into the NOMERGER simulation.

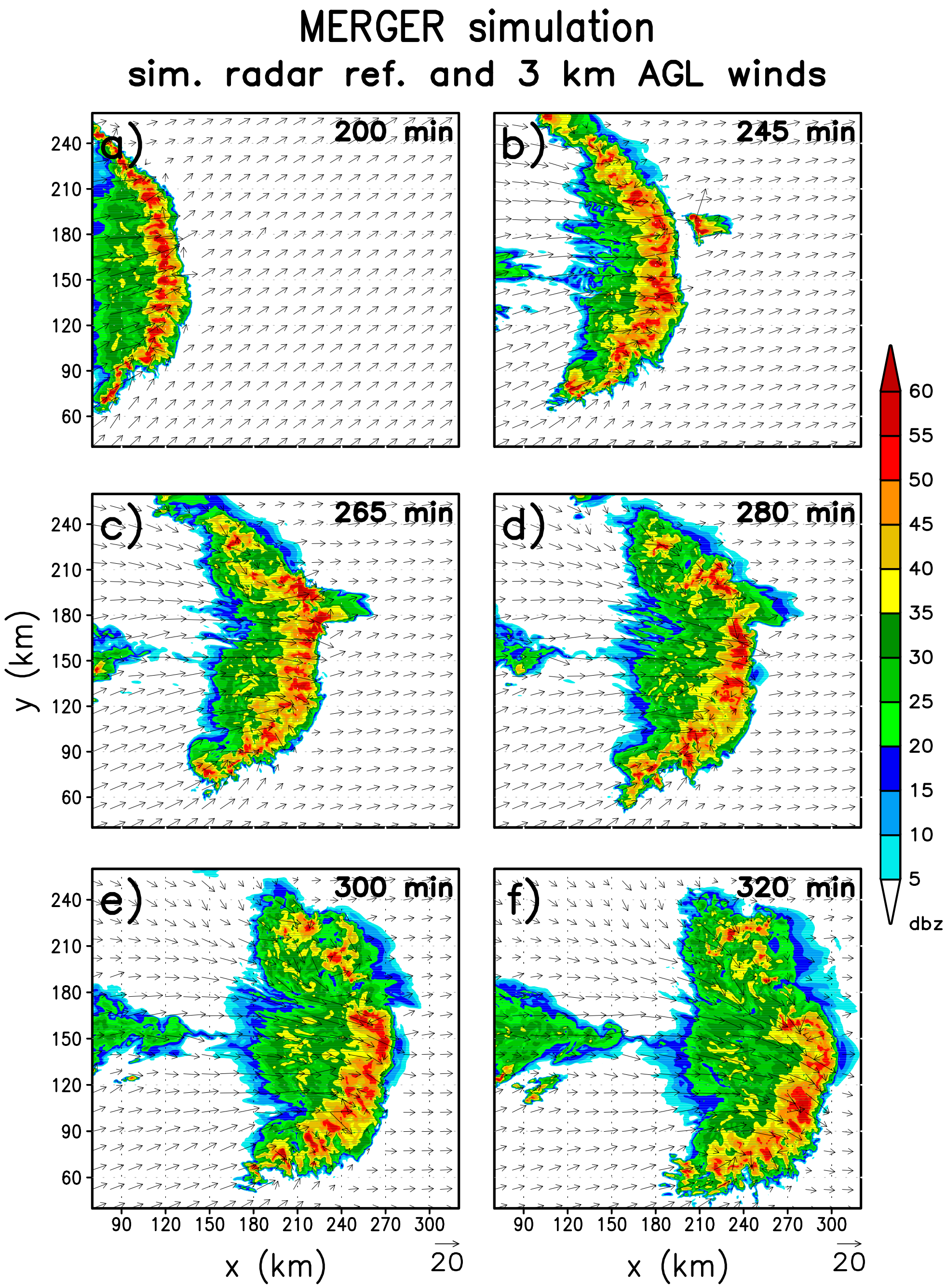

Figure 7: As in Fig. 6, but for the MERGER simulation.

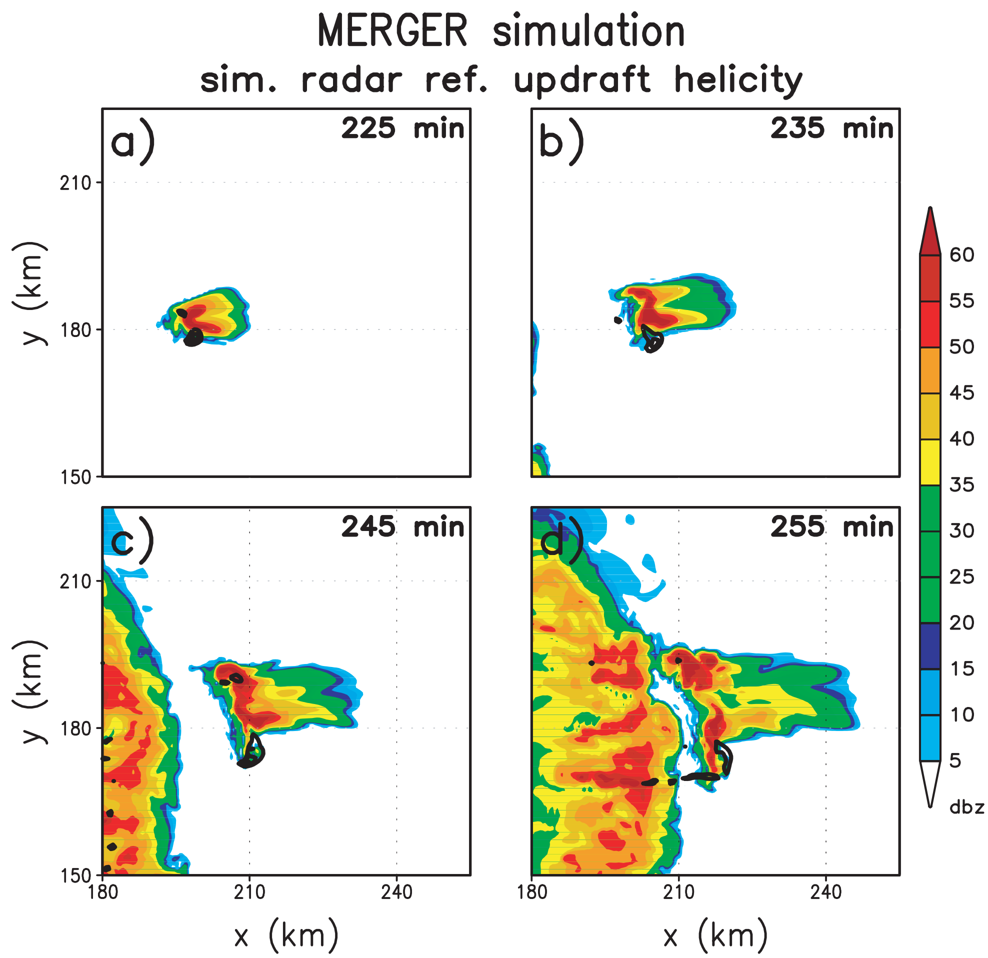

Figure 8: Simulated radar reflectivity (dBZ, shaded as shown) and updraft helicity (contoured every 500 m^2 s^{-2}) associated with the simulated supercell at (a) 225 (b) 235 (c) 245 (d) 255 minutes into the MERGER simulation.

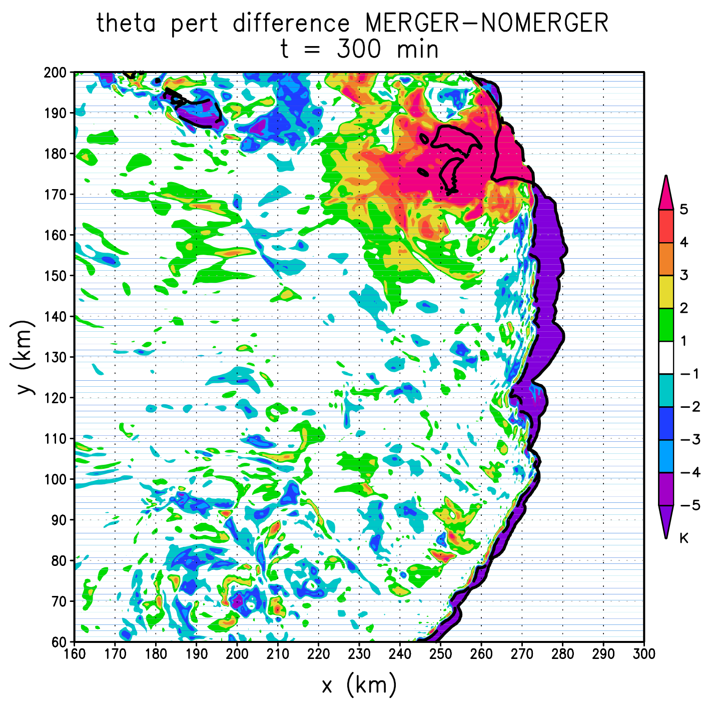

Figure 9: Difference plot comparing the surface potential temperature perturbation (K, shaded as shown) in the MERGER and NOMERGER simulations (MERGER-NOMERGER). The sold and dashed black contours indicate the positions of the -1 K potential temperature contours, representing the gust front location for the MERGER and NOMERGER simulations, respectively.

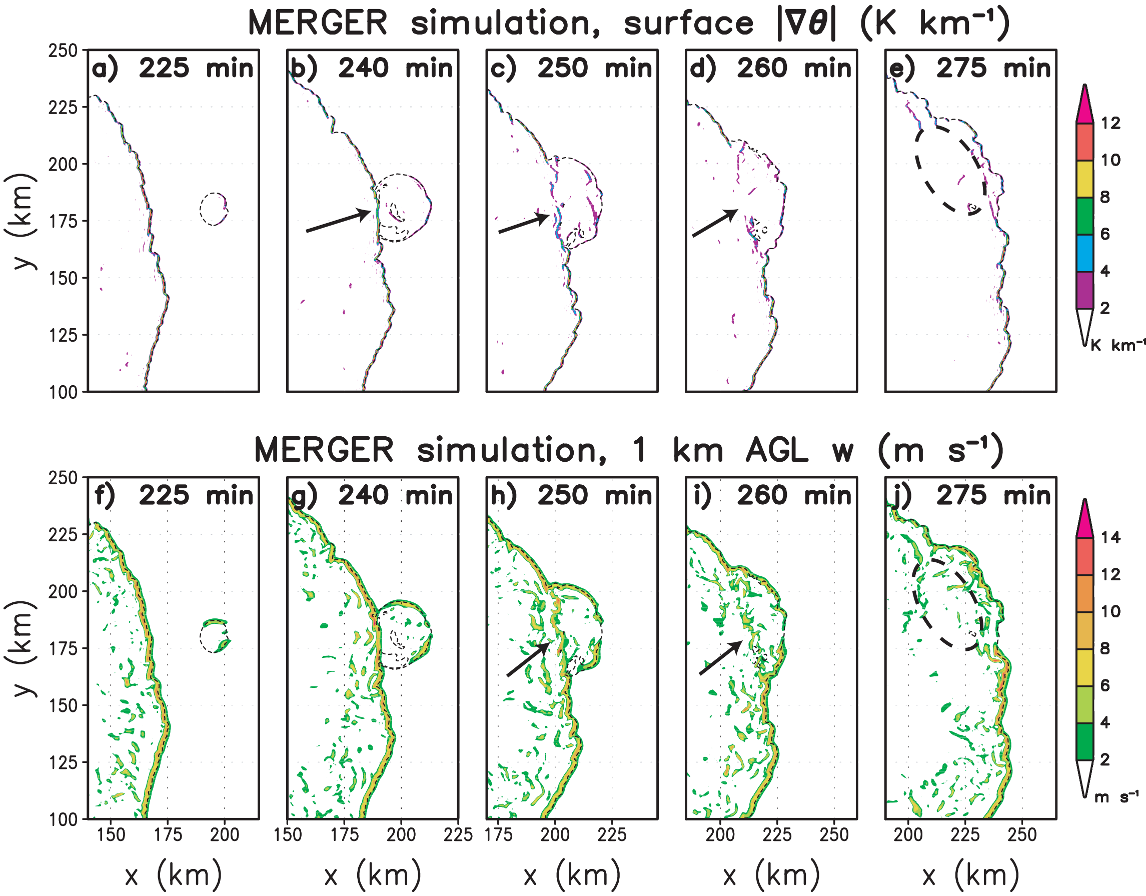

Figure 10: Evolution of gust front lifting in the MERGER simulation. (a-e) magnitude of the surface potential temperature gradient (K km^{-1}, shaded as shown) and -1 K theta perturbation (dashed contour). (j-g) 1 km AGL vertical velocity (m s^{-1}, shaded as shown) and -1 K surface theta perturbation (dashed contour). Arrows and dashed ovals denote features of interest discussed in the text.

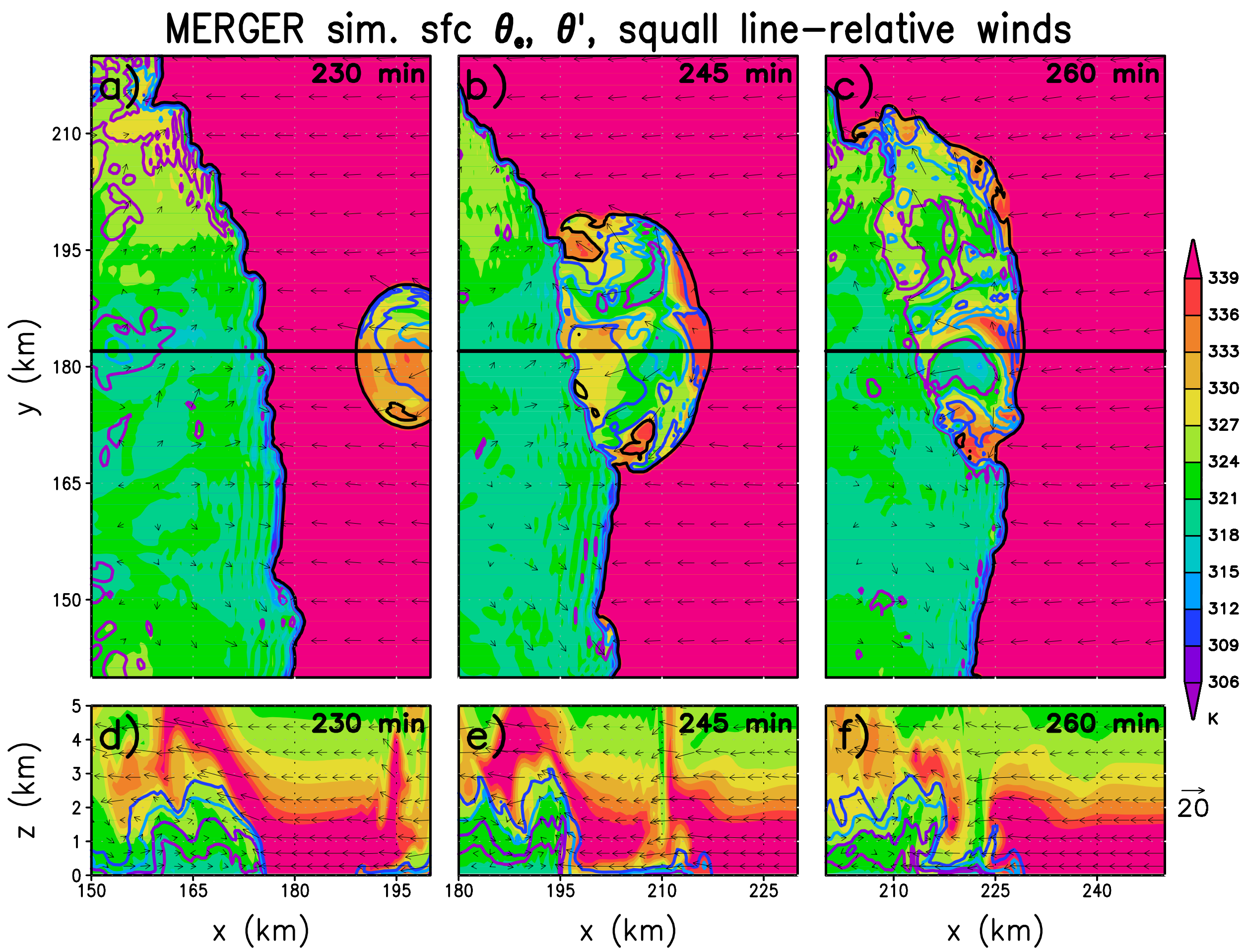

Figure 11: Evolution of storm-relative inflow between t = 230 minutes and t= 260 minutes (left-to-right) in the MERGER simulation. Top panels: plan-view of surface equivalent potential temperature (K, shaded as shown), surface potential temperature perturbation (contoured at -2 (black), -4 (dark blue), -6 (medium blue) and -8 (purple) K, and squall line-relative surface winds. Bottom panels: x-z cross sections of the same fields in as in (a-c) taken along the black lines shown in (a-c).

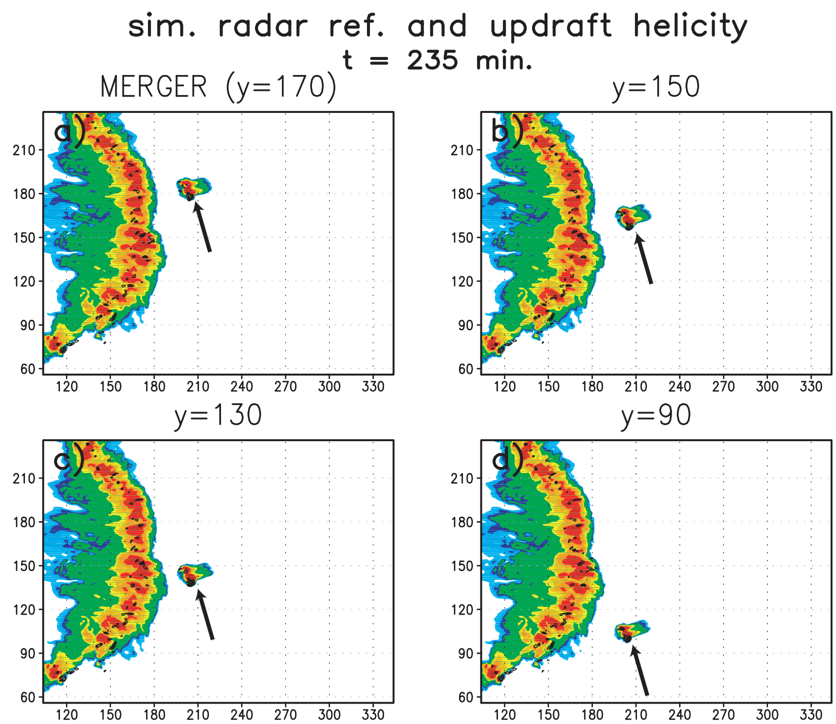

Figure 12: Plan-view plots of simulated radar reflectivity (shaded as shown, dBZ) and integrated updraft helicity (contoured every 250 m^2 s^{-2}) at t = 235 min. for (a) MERGER simulation, (b) Y150 simulation, (c) Y130 simulation, (d) Y90 simulation. Black arrows identify the supercell in each panel.

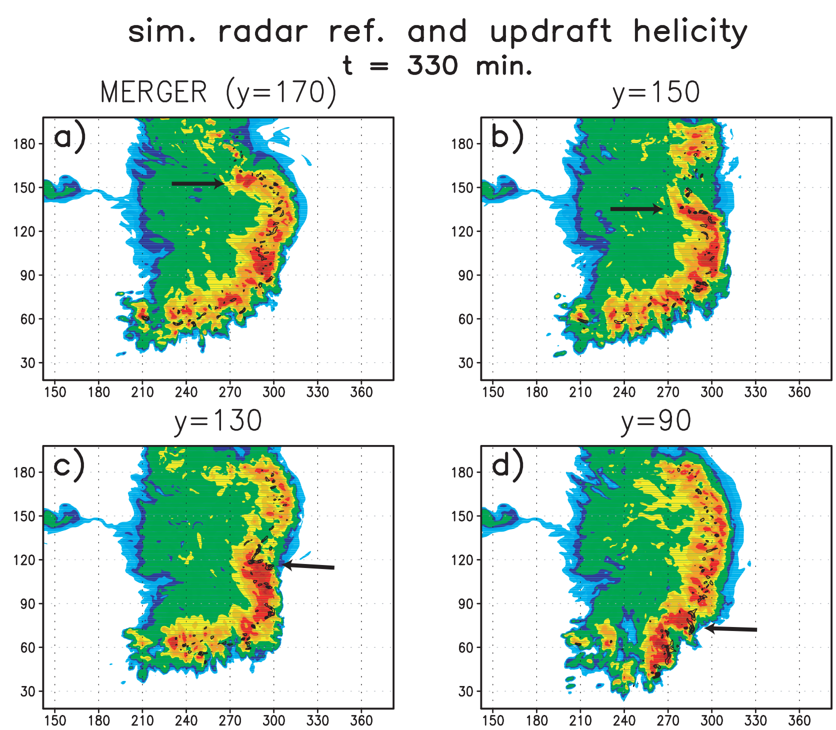

Figure 13: As in Fig. 12 but at t = 330 min. Black arrows identify the location of the merged supercell in each panel.

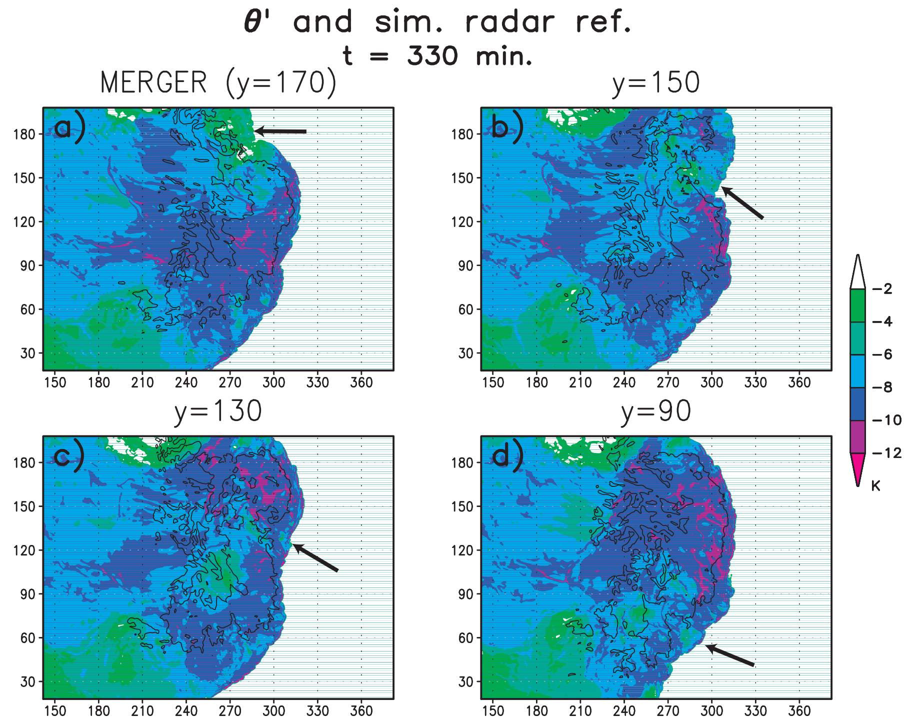

Figure 14: As in Fig. 13 but showing the surface potential temperature perturbation (shaded as shown, K) and the 40 dBZ simulated radar reflectivity contour. Black arrows denote areas of comparatively weaker cold pool in the vicinity of the merger in each simulation.

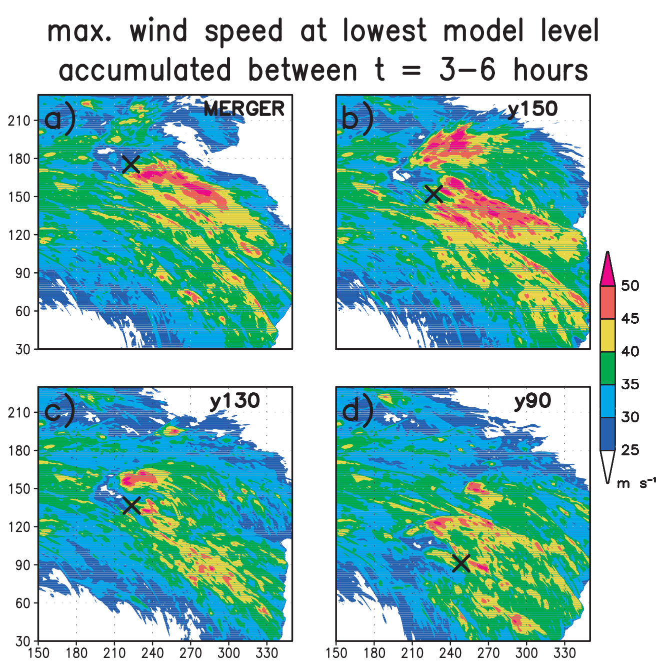

Figure 15: Maximum wind speed at the lowest model level (m s^{-1}, shaded as shown) accumulated between 3 and 6 hours into the simulation for (a) MERGER, (b) Y150, (c) Y130, and (d) Y90 simulations.

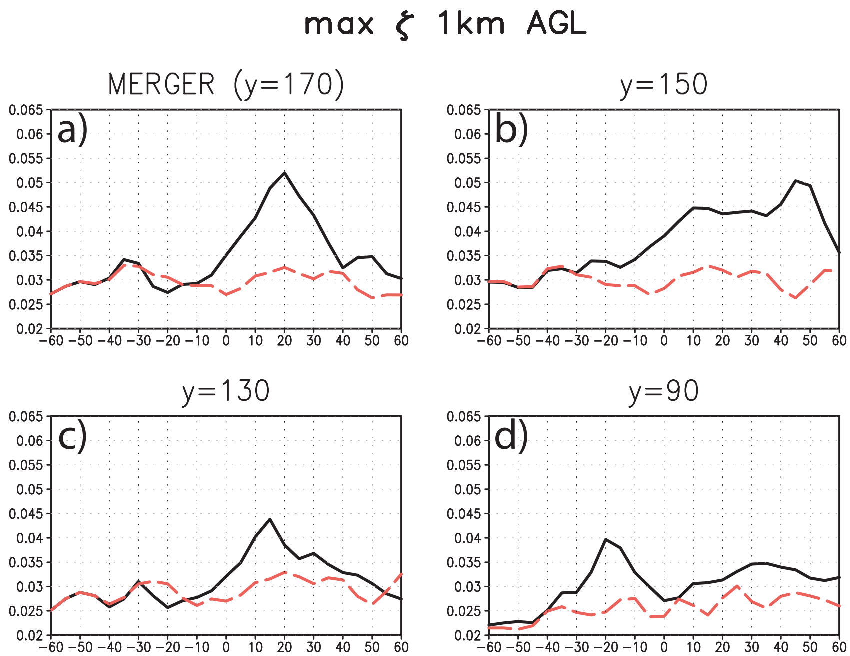

Figure 16: Time-series of maximum vertical vorticity (s^{-1}) calculated at 1 km AGL over 250 km (east-west) by 100 km (north-south) box centered on the merger for (a) MERGER simulation (b) Y150 simulation, (c) Y130 simulation, and (d) Y90 simulation (solid black line). The dashed red line in each panel represents the maximum vorticity calculated over the same region in the NOMERGER simulation.